Modelling anisotropic maturation strains in wood in relation with fibre boundary conditions, microstructure and maturation kinetics

Tancrède Almeras, Joseph Gril, Hiroyuki Yamamoto

Modelling anisotropic maturation strains in wood in relation to fibre boundary conditions, microstructure and maturation kinetics

Tancrède Alméras[1,*], Joseph Gril[2] and Hiroyuki Yamamoto[1]

[1] Laboratory of Bio-material Physics, Graduate School of Bio-agricultural Science, Nagoya University, Chikusa, Nagoya, Japan

[2] Laboratory of Mechanics and Civil Engineering, Faculty of Science, Montpellier University, Montpellier, France

*Corresponding author.
Laboratory of Bio-material Physics, Graduate School of Bio-agricultural Science, Nagoya University, Chikusa, Nagoya 464-8601, Japan
Tel.: +81-52-789-4152
Fax: +81-52-789-4150
E-mail: tancrede@nuagr1.agr.nagoya-u.ac.jp

Abstract

A generalisation of existing mechanical models is proposed to account for the relation between wood macroscopic properties and fibre microstructure and chemical composition. It is applied to understanding of the origin of anisotropic maturation strains measured at the outermost surface of the xylem. Various assumptions are considered for boundary conditions of the fibre during the progressive maturation process and are applied to experimental data from the literature. Assumptions that the fibre is fully restrained in displacement, or fully unrestrained or unrestrained in the transverse direction only are all incompatible with observations. Indeed, within the tree, the fibre is restrained in the longitudinal and tangential directions, but unrestrained in the radial direction towards the bark. Mixed boundary conditions must be introduced to correctly simulate both longitudinal and tangential maturation strains. In the context of an analytical axisymmetric model, this is estimated by considering a parameter of partial release of tangential stress during maturation. Consistence with data and with finite element computation in the case of a square fibre confirmed that, because of the unrestrained radial condition, a large part of the tangential maturation stress is released *in situ*.

Keywords: anisotropy; boundary conditions; cell-wall maturation; growth strain; multilayer model; residual stress; wood fibre.

Introduction

Models relating wood properties to its microstructure have been used to study various wood properties, such as stiffness (Koponen et al. 1989; Harrington et al. 1998; Yamamoto and Kojima 2002; Kojima and Yamamoto 2004b), viscoelasticity (Kojima and Yamamoto 2004a), drying shrinkage (Barber and Meylan 1964; Cave 1972; Yamamoto 1999) and maturation strains (Archer 1987; Yamamoto 1998; Guitard et al. 1999). Early models were based on a rather simple representation of the fibre wall material as a matrix of lignin and hemicellulose reinforced by a cellulosic microfibrillar framework (Barber and Meylan 1964; Cave 1972). Further models integrated increasing realism and complexity. Axisymmetric models (Barber 1968; Archer 1987; Yamamoto 1998, 1999; Sassus et al. 2004) allowed the cylindrical shape of compression wood fibres to be taken into account. Multi-layer models with two, three or four layers were proposed. Finally, the variations of material properties were accounted for using a kinetic description of the transformation process (Yamamoto 1998, 1999). Application of elaborated models allowed a satisfactory description of drying shrinkage and longitudinal maturation strain. However, simulated results for tangential maturation strains were not consistent with observations (Yamamoto 1998).

Because of the evolution of the stiffness of cell wall components, the final state of the fibre cannot be computed by a simple elastic calculation. In this case, the boundary conditions assumed during the transformation process may have an influence on the final state. In most formulations the fibre is assumed to be “virtually isolated”. However, accounting for the real boundary conditions of the fibre may lead to different results. Archer (1987) developed a theoretical model assuming full restraint of the fibre during maturation. He outlined the fact that this assumption is not completely appropriate, because a distinction should be made between the fibre boundary conditions in the radial and tangential directions of the tree, which is not possible in an axisymmetric formulation. The present paper aims at overcoming this limitation by taking a better account of boundary conditions. An explicit general formulation of the fibre model that embraces all previous formulations is provided. It is applied using literature data (Yamamoto 1998) and newly adjusted parameters.

Material and methods

A description of the assumptions and parameters involved in the model is presented in this section. An explicit mathematical presentation can be found online (Alméras et al. 2004b). Some assumptions on which the model is based, although classically used, are subject to discussion (Yamamoto 1998; Guitard et al. 1999; Sassus et al. 2004). Only a discussion on boundary conditions and their consequences is proposed in the present paper.

Modelling wood material

Wood sub-micrometric structure can be described as a framework of microfibrils made of crystalline cellulose, embedded in a matrix of amorphous material consisting of lignins and hemicelluloses. The crystalline framework is assumed to be orthotropic. Its mechanical behaviour here is sufficiently characterised by its longitudinal modulus of elasticity E_l^f. The amorphous matrix is supposed to be isotropic, characterised by its modulus of elasticity E^m and its Poisson ratio ν^m. Both are submitted to induced strains α_l^f and α^m due to the maturation process. Wood material results from a mix of these constituents in volumetric proportions p^f and p^m. Its behaviour is approximated by a simple law of mixture, expressed in the reference system associated to the microfibril. Microfibrils are oriented at an angle ϕ relative to the longitudinal axis of the fibre. The behaviour of wood material in the reference system associated to the fibre is deduced using a tensor rotation formula. Because of the anti-symmetric situation of adjacent fibre walls, full shear restraint is assumed, so that only normal components of the behaviour are kept.

Modelling the wood fibre

The wood fibre is modelled as a cylindrical hollow structure made of n concentric layers. This representation can adapt to the usual description of various fibre types, with an external compound middle lamella (CML), and two or three inner secondary layers (S1, S2, S3 or G). The external radius of the fibre is denoted by r_0. Layers are numbered from the outer side to the inner side of the fibre wall. Each layer is characterised by its inner radius r_i, proportion of microfibrils p_i^f and microfibril angle (MFA) ϕ_i. The stiffness and induced strains are computed using the model of wood material. The strain and stress fields inside the fibre are computed using an analytical solution provided by Archer (1987). The solution depends on the boundary conditions imposed on the fibre. They are defined at three bounds: the longitudinal bound, the internal radial bound and the external radial bound. The internal radial bound is assumed to be stress-free, meaning that the internal pressure of the living cell is neglected. For each of the other bounds, two options are considered. They may be assumed to be either fully restrained or fully unrestrained in displacement. The main outputs of the model are parameters describing the state of the fibre at its external bounds: radial displacement $u_r(r_0)$, radial stress $\sigma_r(r_0)$, longitudinal strain ε_z and longitudinal load N.

Modelling maturation kinetics

The maturation of a wood fibre is a progressive process that occurs together with the deposition of cell wall material. The amount of constituents, and therefore their stiffness, increases at the same time as maturation strains are induced. Because the stiffness is not constant, the above elastic model cannot be directly used to compute the final state of the fibre. Analytical formulation and resolution of the model with variations of stiffness were not explicitly carried out. We used a numerical method instead. Maturation was divided into a finite number of elementary steps. The stiffness of the constituents increases between steps, and is assumed to be constant during a step. At each step, an elementary increment of strain is induced in the constituents, and the elastic model is used to compute the output parameters. These are cumulated to compute the final state of the fibre.

Modelling maturation strains

During maturation, strains are progressively induced at the level of the constituents. This results in a potential maturation strain at the level of the fibre. Due to physical restraints (depending on the boundary conditions of the fibre), only part of this strain is expressed (i.e., actually achieved) during the maturation process, and the other part is accumulated as maturation stress. This accumulated part can be artificially released at the xylem surface. Released strains are measured using various methods (Yoshida and Okuyama 2002) by cancelling longitudinal and tangential maturation stress either independently (denoted by ε_L and ε_T) or together (in this case called "LT-released" strains, denoted by ε_L^* and ε_T^*). Classically, the expressed part of the maturation strain is considered negligible, so that released strain is considered to be equal to maturation strain.

Two points of view are considered in the present paper. The first consists of modelling maturation of the fibre inside the tree. Discussing the assumptions for the boundary conditions of the fibre in this context is the objective of the present paper. In this case, maturation results in maturation stresses $\sigma_r(r_0)$ and/or N. Strains released independently (ε_L, ε_T) or simultaneously (ε_L^*, ε_T^*) can be easily computed with the wood fibre model using a single elastic step with imposed boundary stresses $\sigma_r(r_0)$ and/or $-N$. The second point of view is referred to as the "virtually isolated fibre" assumption. In this case, calculation at the fibre level is performed assuming that boundary conditions during maturation are unrestrained in both the longitudinal and radial directions. Then, the stresses computed by the model at the boundaries [$\sigma_r(r_0)$ and N] vanish, because all maturation strains are expressed during maturation. These expressed strains, ε_z and $u_r(r_0)/r_0$, are then supposed to be equal to the released strains ε_L^* and ε_T^* measured at the tree level.

Reference model and data

A recent application of the wood fibre model was performed by Yamamoto (1998). In this paper, the author studied the relation between MFA and maturation strains (as well as other wood properties). His model is assessed on data measured on 44 samples of sugi (*Cryptomeria japonica* D. Don) late wood. The MFA of the S2 layer was measured by X-ray diffraction. Released maturation strains were measured with strain gages in the T and L directions, after complete release in both directions. The present model is similar to Yamamoto's model in many aspects. The fibre structure is represented as embedded concentric layers, and each layer is assumed to consist of a matrix of lignin and hemicellulose reinforced with a cellulose framework, both submitted to kinetic variations of stiffness and induced strains. Mathematical formulation and resolution are slightly different, but both models are based on mostly identical mechanical and structural assumptions. The main difference is the distinction between "maturation" and "released" strains, related to the boundary conditions of the fibre. In Yamamoto's model the "virtually isolated fibre" assumption is made. In the present model, this assumption is an option, and other conditions are explored.

Evaluation and optimisation of the model

A simulation was performed with the same parameters used by Yamamoto (1998). This provides a numerical cross-validation of both models and is considered as a reference for the examination of other assumptions. The reference set of parameters describes a typical fibre of sugi late wood. Input parameters of the model describe the structure of the fibres, the mechanical properties of its elementary constituents, induced strain in each constituent and the kinetics of the maturation process. Output parameters are simulated values of ε_L^* and ε_T^* for various values of MFA inside the S2 layer. Most input parameters are set to fixed values. In particular simulations, some parameters (p) (Table 2) are adjusted to fit the observed data using a least-

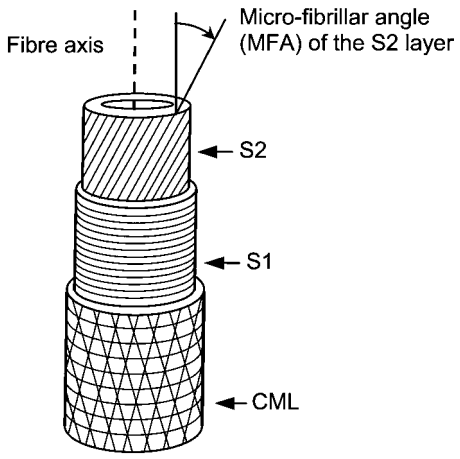

Figure 1 Schematic representation of a wood fibre.

square method by minimising the distance D between simulations and observations:

$$D(p)=\Sigma_{obs}(w_L[\varepsilon_L{}^*(p,\phi^{obs})-\varepsilon_L^{obs}]^2+(1-w_L)[\varepsilon_T{}^*(p,\phi^{obs})-\varepsilon_T^{obs}]^2)$$

where $\varepsilon_L{}^{obs}$, $\varepsilon_T{}^{obs}$ and ϕ^{obs} are data measured for a given observation and w_L is the weight of the longitudinal strain. It is set to 0.5 when attempting to fit both $\varepsilon_L{}^{obs}$ and $\varepsilon_T{}^{obs}$, and to 0 or 1 when concentrating on $\varepsilon_T{}^{obs}$ or $\varepsilon_L{}^{obs}$ singly.

Parameter set

Fibre structure The fibre is supposed to consist of three main layers (CML, S1 and S2) (Figure 1). The effect of the S3 layer is neglected. Parameters for each layer's structure are given in Table 1. These are representative values, based on direct measurements of the fibre structure and chemical composition. In the case of Yamamoto's simulation, the CML was assumed to be isotropic. In order to simulate the same situation while maintaining consistency with our description of the other layers, we assumed that the MFA was 0° for 1/4 of the framework, 90° for another 1/4 and 45° for the remaining half. The MFA inside the S2 layer is a variable parameter and was set at successive values between 0° and 45° during simulations.

Maturation kinetics Based on literature observations (Terashima 1990), the maturation kinetics inside the cell wall was assumed to progress as follows: (1) completion of the CML rigidity and deposition of the cellulose microfibrils in the secondary layers; (2) progressive lignification of the S1 layer, increasing the stiffness of its matrix fraction and induced strains in both constituents; and (3) similar progressive lignification of the S2 layer. During each step, stiffness and induced strains of the maturing layer are supposed to increase with time from 0 to their maximal value.

Elastic constants Values of the longitudinal elastic modulus of cellulose (134 GPa) and isotropic elastic modulus of the matrix (2 GPa) are based on experimental works (Sakurada et al. 1962; Cousins 1976) and on consistency with macroscopic data on wood stiffness. The Poisson ratio of the matrix substance was set close to 0.5, to conform to Yamamoto's assumption of incompressibility. Impact of this assumption is tested by adjusting this parameter. All other stiffness parameters were neglected in Yamamoto's calculation and are set here to values close to 0.

Induced strains In accordance with Yamamoto (1998), we assumed that the strain induced by maturation involves swelling inside the matrix and shrinkage inside the framework. Values of induced strains in the constituents cannot be observed directly. Yamamoto fitted them in order to obtain the best agreement between data and simulations. The shrinkage induced in the framework was assumed to be identical (−0.15%) inside the S1 and S2 layers. Expansion of the matrix substance inside the S2 layer (+0.5%) was supposed to be half that in the S1 layer (+1%). This assumption is based on the consideration that the degree of maturation is lower in the S2 layer, due to its lower lignification. These values were used as a reference for the simulations before trying new adjustments. Induced strains inside the CML were neglected.

Table 1 Structure and chemical composition of the concentric layers constituting the fibre.

Layer	Thickness (%)	Framework (%)	Matrix (%)	MFA
CML	2.4	15	85	0°/45°/90°
S1	8.9	15	85	90°
S2	29.6	30	70	0°–45°

Thickness of the layers is expressed as percentage of the fibre radius. Microfibril angle (MFA) of the CML layer is 0° for 1/4, 90° for 1/4, and 45° for 1/2 of the framework. MFA of the S2 layer takes successive values between 0° and 45° in simulations.

Results

Boundary conditions assumptions

Virtually isolated fibre Longitudinal and tangential maturation strains simulated under this assumption are shown in Figure 2 as a function of the MFA of the S2 layer. Dotted lines indicate Yamamoto's original results. Simulated $\varepsilon_L{}^*$ is −0.09% for MFA=0°. This increases exponentially up to +0.17% for MFA=40°. A longitudinal release strain of 0% is obtained for MFA=27°. Simulated $\varepsilon_T{}^*$ is +0.27% for MFA=0° and decreases to +0.16% for MFA=40°. The shape of the curves is similar to Yamamoto's, with slightly lower values for $\varepsilon_L{}^*$ and higher values for $\varepsilon_T{}^*$. These small discrepancies between the models are related to minor differences in the implementation, with some second-order terms neglected in Yamamoto's formulation and accounted for in the present one. Simulation gave fairly good results for $\varepsilon_L{}^*$, but overestimated values for $\varepsilon_T{}^*$. Attempts to correct this bias by

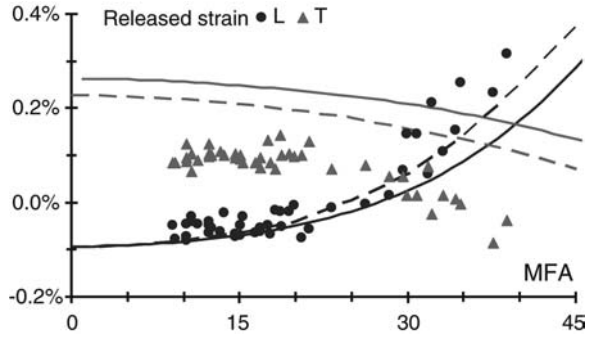

Figure 2 Longitudinal (L) and tangential (T) maturation strains simulated for a virtually isolated fibre with the present model (solid lines) and with Yamamoto's model (dotted lines), using Yamamoto's parameters. Points represent measurements of released strains from Yamamoto (1998).

Table 2 Values of induced strains, Poisson's ratio and release coefficient for the simulations.

Boundary condition	Optimisation	α_l^f (%)	α^m (%)	ν^m	k_T
Isolated fibre (unrestrained)	Yamamoto (L)	0.15	1.00	0.5	1
	L.S. (T)	0.06[a]	0.39[a]	0.5	1
	L.S. (L and T)	0.14[a]	1.89[a]	0.37[a]	1
Fully restrained	L.S. (L and T)	0.05[a]	0.47[a]	0.46[a]	0
Transversely unrestrained	L.S. (T)	0.32[a]	1.38[a]	0.5	1
Partial release	L.S. (L and T)	0.15	1.00	0.5	0.67[a]
	L.S. (L and T)	−0.16[a]	1.53[a]	0.49[a]	0.26[a]

[a]Parameters adjusted by the least square (L.S.) optimisation procedure targeting L and/or T data (other are imposed values).

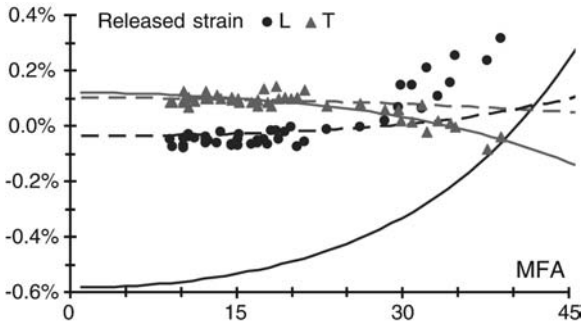

Figure 3 Longitudinal (L) and tangential (T) maturation strains simulated for a virtually isolated fibre, after optimisation of induced strains and Poisson's ratio, targeting T data only (solid lines) or T and L data together (dotted lines). Points represent measurements of released strains from Yamamoto (1998).

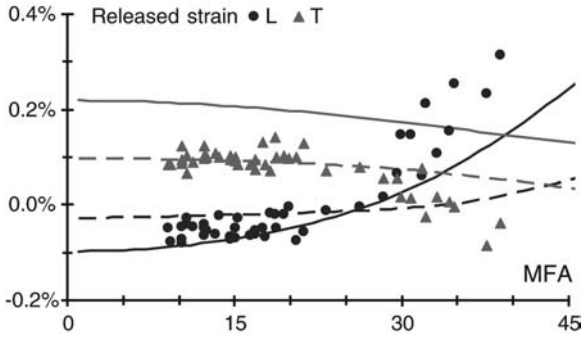

Figure 4 Longitudinal (L) and tangential (T) maturation strains simulated assuming full displacement restraint, using Yamamoto's parameters (solid lines) and after optimisation of induced strains and Poisson's ratio targeting all data (dotted lines). Points represent measurements of released strains from Yamamoto (1998).

adjusting values of induced strains in the constituents α_l^f, α^m and Poisson's ratio of the matrix ν^m (Table 2) failed to fit both ε_T^* and ε_L^* for all MFAs. No significant improvement to ε_T^* results could be achieved without decreasing agreement with ε_L^* (Figure 3). This suggests that the quality of the model is not limited by these parameters, but may be limited by the boundary condition assumptions.

Full restraint A simulation was performed assuming that the fibre was fully restrained during maturation (Figure 4). For MFA $<25°$, the simulated released strains are similar to those obtained for the virtually isolated fibre. For higher MFAs, ε_T^* have slightly higher values and ε_L^* lower values. Adjusting α_l^f, α^m and ν^m (Table 2) did not lead to satisfactory results for both data series (Figure 4).

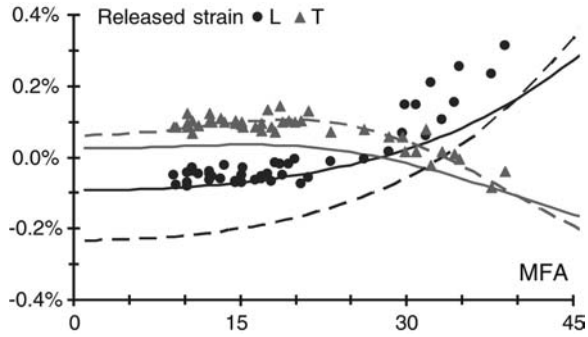

Figure 5 Longitudinal (L) and tangential (T) maturation strains simulated assuming the fibre is longitudinally restrained and transversely unrestrained, using Yamamoto's parameters (solid lines) and optimised induced strains targeting T-data (dotted lines). Points represent measurements of released strains from Yamamoto (1998).

No restraint in the transverse plane A third set of simulations was performed assuming that the fibre was fully restrained in its longitudinal direction but unrestrained in its transverse plane. In this case, no transverse stress is accumulated during fibre maturation, because the fibre was assumed to strain freely in the transverse plane. Then, ε_T^* is only a consequence of coupling with the release of longitudinal strains. Using Yamamoto's parameters, results for ε_L^* are similar to those obtained with previous assumptions and in agreement with the data (Figure 5). However, the variation of ε_T^* differs from other simulations. Values are close to 0.03% for MFA $<25°$ and are negative for higher MFA, reaching -0.12% for MFA $=40°$. These are closer to observations than in previous simulations. They are still lower than the observed data, but the order of magnitude and evolution with MFA is correctly simulated. Induced strains and Poisson's ratio were adjusted to fit data with these boundary conditions (Table 2). Agreement for ε_T^* strains could be improved, but in this case agreement for ε_L^* was severely decreased (Figure 5).

Evidence for intermediate boundary conditions Results shown in Figures 2–5 show that boundary conditions do not have major consequences on the simulation of ε_L^*. However, they do have a strong effect on ε_T^*. Assuming unrestrained conditions in the transverse plane improved the agreement with observations for ε_T^* without decreasing it for ε_L^*. However, ε_T^* seems to be limited to values lower than observed if consistency with ε_L^* is imposed. Indeed, in this case, it is assumed that no transverse stress is accumulated during maturation, so that ε_T^* is only due to coupling with ε_L^*. This is why zero

released strain is obtained for both T and L at the same MFA (note, however, that the relation between ε_T^* and ε_L^* is not a simple proportionality, since the ratio depends on the MFA). Therefore, a larger value of ε_T^* for low MFA could be obtained only for a larger absolute value of ε_L^*, which is then inconsistent with the data. Thus, with these boundary conditions, it is virtually impossible to improve agreement for ε_T^* without decreasing it for ε_L^*.

Results for fully restrained or unrestrained radial bounds at the fibre level suggest that the situation for the observed data is between these two assumptions. Other direct arguments support this idea. Strains released tangentially without longitudinal release (defined as ε_T) are usually not zero, showing that ε_T^* should not be due only to coupling with ε_L^*, but also to radial stress accumulated during fibre maturation. This is not compatible with the assumption of unrestrained radial bounds. Data reported in this paper were obtained in LT-release. The fact that positive values of ε_T^* are observed for null values of ε_L^* also supports this idea. Inside the tree, the condition of the maturing wood fibre is not homogeneous in the transverse plane. It is almost completely blocked in the direction tangential to the tree (T) because of the core of mature wood. However, in the radial direction of the tree (R) it is almost completely unrestrained (the effect of bark being neglected). We suggest that tangential strains cannot be correctly simulated without considering the fact that transverse bounds of the fibre are neither completely restrained nor completely unrestrained.

Partial release of tangential maturation stress during maturation

Because of the assumption of axisymmetry, the distinction between the tree radial and tangential directions cannot be made at the fibre level. Both refer to the radial direction with reference to the axisymmetric fibre model. In this section, we try to overcome this limitation of the cylindrical fibre model while keeping the assumption of axisymmetry. It is assumed that the fibre radial bound is partly blocked and partly free. For this purpose, we consider the partial release of radial stress at the fibre level during maturation, supposed to be achieved through the macroscopic radial direction.

Implementation of partial release during maturation Simulations shown in this section are based on the same parameters and data as above, with a modified version of the model. The change only concerns the boundary conditions of the fibre and the mechanism of stress accumulation. In this implementation, it is assumed that a fraction of the transverse maturation stress is released during the maturation process, and the other fraction is accumulated until final release. The fraction released during maturation is managed by a parameter called the coefficient of transverse stress release (k_T). This parameter has a value between 0 and 1. A value of 0 is equivalent to full displacement restraint and a value of 1 is equivalent to the unrestrained assumption. Intermediate values simulate partial stress release. It is simulated by inserting an "elastic release" step after each elementary maturation step, which consists of cancelling a fraction k_T of the stress accumulated during the previous maturation step.

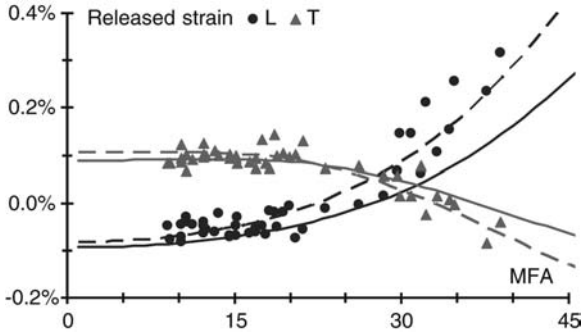

Figure 6 Longitudinal (L) and tangential (T) maturation strains simulated assuming partial stress release in the transverse plane, with Yamamoto's parameters and optimised release coefficient (solid lines) and with optimised induced strains and release coefficient (dotted lines). Points represent measurements of released strains from Yamamoto (1998).

Fitting the coefficient of transverse release The release coefficient is an abstract concept designed to overcome the limitations of the cylindrical model. Its value cannot be directly measured. Therefore, it was adjusted in order to fit the data. Adjusting both the release coefficient and induced strains (Table 2) improved the agreement between simulations and observations when compared to other boundary conditions (Figure 6). Simulated released strains here are correct for both T and L. The value of k_T suggests that a large part (74%) of the transverse stress induced in the fibre wall is released during maturation. Using Yamamoto's induced strains, an optimal value of k_T (0.67) also leads to fairly good results (Figure 6), showing that it is this coefficient, rather than new values of induced strains, that improves the agreement with observed data.

Finite element computation The real situation of the fibre is complete restraint in the macroscopic T direction. However, stress accumulated in the T direction is partly released at the fibre level by transfer to the free R direction. For a correct account of this problem, a non-axisymmetric model is needed. The loss of symmetry leads to complicated formulations, so that the derivation of analytical models becomes rather intractable. However, a finite element calculation is possible. This was performed with CAST3M software for a fibre with square cross-section. The walls of the fibre were assumed to have the same multi-layer structure and stiffness as for the cylindrical model, for MFA = 20°. The corners were assumed to consist of the same substance as the CML. Maturation strains were induced inside the constituents. Two elastic calculations were performed: the first assuming full restraint at external bound on the four sides, and the second assuming that the external tangential wall was unrestrained, while the three other sides were restrained (Figure 7). The profile of the tangential stress along a radial wall was computed in each case.

The fibre shape is clearly modified by the absence of restraint on one side. Consequences are dilatation and ovalisation of the lumen, and a loss of symmetry. The

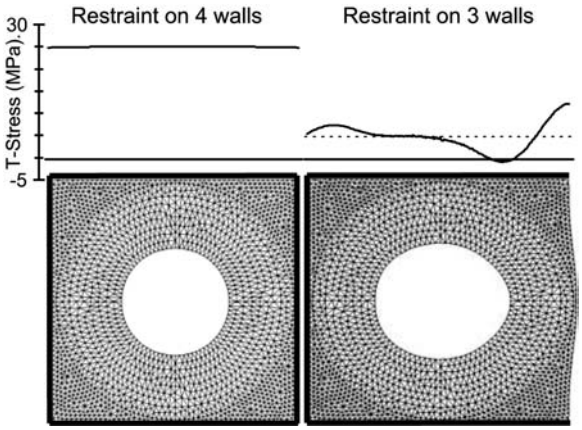

Figure 7 Finite element computation for a square fibre with three or four walls restrained in displacement and submitted to induced strains. Resulting strains were magnified 10-fold for easier visualisation; tangential compression stress along radial walls (solid lines) and mean stress level (dotted lines).

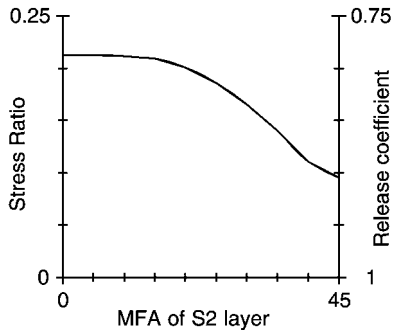

Figure 8 Evolution of the ratio $r_{3/4}$ (tangential stress with three walls restrained over tangential stress with four walls restrained) and the release coefficient $k_T = 1 - r_{3/4}$, computed using finite elements on a square fibre, as a function of the MFA of the S2 layer.

profile of tangential compression stress along a radial wall is almost uniform in the case with four sides restrained. In the case with three sides restrained, the stress is partly transferred to the R direction, resulting in a lower stress level on the radial walls. Heterogeneity of the tangential stress also appears along the radial wall. The mean stress level is much lower than in the four-sides case. The ratio between the three-sides and four-sides cases is $r_{3/4} = 0.21$, meaning that the fraction of released tangential stress ($k_T = 1 - r_{3/4}$) is 0.79 in this case. This fraction should be compared with the adjusted release coefficient $k_T = 0.74$. Additional simulations (Figure 8) showed that the released fraction increases up to 0.9 with the MFA of the S2 layer, tending to almost complete stress release. This evolution may be related to the ratio of transverse stiffness of the S2 and CML layers. Indeed, for large MFAs, the S2 layer is stiffer in the transverse direction, so that strain induced into it strongly pushes on the CML layer, allowing a greater rate of ovalisation and stress transfer.

Discussion

Boundary conditions were shown to have major consequences on the simulated tangential strain. This is related to the fact that the model integrates a kinetic evolution of the constituent's stiffness. Because of the variation of the constituent's stiffness during the maturation process, the calculation of final maturation strains is not elastic. This is easily shown by considering the stress increment σ_1 induced in an early lignification stage t_1, when the wall rigidity is C_1. If no restraint is considered, the stress induced in the new layer generates a strain $\varepsilon_1 = C_1^{-1}\sigma_1$. In the case of full restraint, the same stress σ_1 is blocked until final release time t_n, when the wall rigidity is C_n. The strain generated by the liberation of this stress is therefore $\varepsilon_1' = C_n^{-1}\sigma_1$. As the rigidity increases with time ($C_n > C_1$), we have $\varepsilon_1' < \varepsilon_1$. This result is analogous to those obtained in tree biomechanics (Castera and Morlier 1991; Fournier et al. 1991; Alméras et al. 2004a) showing that the strains and stress inside a tree stem depend not only on its dimensions, elastic properties and load, but also on the history of these parameters. The influence of longitudinal boundary conditions is low because the cellulose is assumed to be already stiff at the beginning of maturation. Cellulose mainly acts as longitudinal reinforcement, so that the relative variation of longitudinal stiffness due to lignification is low and the elastic solution is a good approximation in the longitudinal direction.

In the case of an elastic calculation, the expressed strain of a virtually isolated fibre would be equivalent to the released strain of a fully restrained fibre. As the calculation is not elastic, this is no longer equivalent. The assumption of a virtually isolated fibre was used successfully for modelling drying shrinkage, also in a non-elastic context (Yamamoto 1999). However, in this case, the assumption of free bounds was justified because, when a piece of wood is dried, induced strain is actually expressed instead of being accumulated and released in the final state. For the simulation of maturation strains, other boundary conditions must be considered. Guitard et al. (1999) obtained good agreement for tangential strains under the virtually isolated fibre assumption, using the same data and slightly different parameters. Many basic assumptions of this model are similar to the present one, but the validity of the mechanical resolution is questionable. Indeed, the "local condition" used in their Eq. (20) simplifies much the mathematical resolution, but is not compatible with the assumption of plane strains used in their Eq. (14). The solution therefore does not seem to be completely sound from a mechanical point of view.

Using a rigorous solution, we could obtain good agreement between observations and simulations by introducing partial release of the transverse stress during maturation. Some parameters were adjusted using a method that ensures convergence to the optimal values. The fact that adjusted induced strains are close to those obtained by Yamamoto (1998) using a "trial and error" method confirms that improvement of the simulation is due to a better account of boundary conditions rather than to a change in postulated induced strains. The adjusted value of the release coefficient is consistent with the released fraction computed in a non-axisymmetric case. This parameter allowed retention of the cylindrical formulation of the mechanical problem, while accounting

for the fact that the fibre is not fully restrained in the transverse plane. The possibility of accounting for boundary stresses during a non-linear transformation process opens new perspectives of applications for modelling various phenomena or technological processes at the fibre level, such as wood bending, forming, drying under restraint or mechano-sorption. Further study of maturation strains with this tool includes analysis of the coupling between longitudinal and tangential strains, and modelling of the interaction between fibre maturation and day/night changes in tree diameter.

References

Alméras, T., Costes, E., Salles, J.C. (2004a) Identification of biomechanical factors involved in stem shape variability between apricot-tree varieties. Ann. Bot. 93:1–14.

Alméras, T., Gril, J., Yamamoto, H. (2004b) Modelling anisotropic maturation strains in wood in relation with fibre boundary conditions, microstructure and maturation kinetics: mechanical formulation of the fibre model. http://www.lmgc.univ-montp2.fr/~jgril/hf/.

Archer, R.R. (1987) On the origin of growth stresses in trees. Part 1. Micromechanics of the developing cambial cell wall. Wood Sci. Technol. 21:139–154.

Barber, N.F. (1968) A theoretical model of shrinking wood. Holzforschung 22:97–103.

Barber, N.F., Meylan, B.A. (1964) The anisotropic shrinkage of wood: a theoretical model. Holzforschung 18:146–156.

Castera, P., Morlier, V. (1991) Growth patterns and bending mechanics of branches. Trees 5:232–238.

Cave, I.D. (1972) Swelling of a fibre-reinforced composite in which the matrix is water-reactive. Wood Sci. Technol. 6:157–161.

Cousins, W.J. (1976) Elastic modulus of lignin as related to moisture content. Wood Sci. Technol. 10:9–17.

Fournier, M., Chanson, B., Thibaut, B., Guitard, D. (1991) Mechanics of standing trees: modelling a growing structure subjected to continuous and fluctuating loads. 2. Three-dimensional analysis of maturation stresses in a standard broad-leaved tree. Ann. For. Sci. 48:527–546.

Guitard, D., Masse, H., Yamamoto, H., Okuyama, T. (1999) Growth stress generation: a new mechanical model of the dimensional change of wood cells during maturation. J. Wood Sci. 45:384–391.

Harrington, J.J., Booker, R., Astley, R.J. (1998) Modelling the elastic properties of softwood. Part 1: the cell-wall lamellae. Holz Roh- Werkstoff 56:37–41.

Kojima, Y., Yamamoto, H. (2004a) The effect of microfibril angle on the longitudinal tensile creep behavior of wood. J. Wood Sci. 50:301–306.

Kojima, Y., Yamamoto, H. (2004b) Properties of the cell wall constituents in relation to the longitudinal elasticity of wood. Part 2: origin of the moisture-dependency of the longitudinal elasticity of wood. Wood Sci. Technol. 37:427–434.

Koponen, S., Torati, T., Kanerva, P. (1989) Modelling longitudinal elastic and shrinkage properties of wood. Wood Sci. Technol. 23:55–63.

Sakurada, I., Nukushima, Y., Ito, T. (1962) Experimental determination of the elastic modulus of crystalline regions in oriented polymers. J. Polymer. Sci.

Sassus, F., Alméras, T., Gril, J., Yamamoto, H. (2004) Modélisation des déformations de maturation de la fibre. Cah. Sci. Bois (in press).

Terashima, N. (1990) A new mechanism for the formation of a structurally ordered protolignin macromolecule in the cell wall of tree xylem. J. Pulp Pap. Sci. 16:150–155.

Yamamoto, H. (1998) Generation mechanism of growth stresses in wood cell walls: roles of lignin deposition and cellulose microfibril during cell wall maturation. Wood Sci. Technol. 32:171–182.

Yamamoto, H. (1999) A model of the anisotropic swelling and shrinking process of wood. Part 1: generalisation of Barber's wood fibre model. Wood Sci. Technol. 33:311–325.

Yamamoto, H., Kojima, Y. (2002) Properties of the cell wall constituents in relation to the longitudinal elasticity of wood. Part 1: formulation of the longitudinal elasticity of an isolated wood fiber. Wood Sci. Technol. 37:427–434.

Yoshida, M., Okuyama, T. (2002) Techniques for measuring growth stress. Holzforschung 56:461–467.

Modelling anisotropic maturation strains in wood in relation with fibre boundary conditions, microstructure and maturation kinetics

Tancrède ALMÉRAS[1], Joseph GRIL[2], Hiroyuki YAMAMOTO[1]

1: Laboratory of bio-material physics, Graduate School of bio-agricultural science, Nagoya University (Chikusa, Nagoya 464-8601, Japan)

2: Laboratory of mechanics and civil engineering, Faculty of science, Montpellier University (CC048, Place Eugène Bataillon, 34095 Montpellier Cedex 5, France)

Appendix: mechanical formulation of the fibre model

Mechanical behaviour of elementary constituents

The matrix of amorphous material is assumed isotropic and denoted with superscript *m*. Its mechanical behaviour is characterized by its Young's modulus E^m, Poisson's ratio ν^m, shear modulus $G^m = E^m/[2(1+\nu^m)]$ and induced strain α^m. The framework of crystalline material (superscript *f*) is assumed transverse isotropic, associated to the reference "*ttl*", where *l* is the direction of microfibrils and the direction *t* transverse to them. Its mechanical behaviour is characterized by its longitudinal and transverse Young's moduli (E_l^f , E_t^f), Poisson's ratios (ν_{tl}^f, ν_{tt}^f), shear moduli (G_{tl}^f, G_{tt}^f) and induced strains (α_l^f, α_t^f).

Both constituents of the wood material are assumed to have an elastic behaviour with induced strains, defined in *ttl* by the relation between the stress vector $\underline{\sigma}$ and strain vector $\underline{\varepsilon}$:

$$\underline{\sigma}^m = \underline{\underline{C}}^m(\underline{\varepsilon}^m - \underline{\alpha}^m) \quad (1\text{-a})$$

$$\underline{\sigma}^f = \underline{\underline{C}}^f(\underline{\varepsilon}^f - \underline{\alpha}^f) \quad (1\text{-b})$$

Stiffness matrices, $\underline{\underline{C}}^m$ and $\underline{\underline{C}}^f$ are:

$$\left(\underline{\underline{C}}^{m}\right)^{-1} = \begin{bmatrix} \frac{1}{E^m} & \frac{-\nu^m}{E^m} & \frac{-\nu^m}{E^m} & 0 & 0 & 0 \\ \frac{-\nu^m}{E^m} & \frac{1}{E^m} & \frac{-\nu^m}{E^m} & 0 & 0 & 0 \\ \frac{-\nu^m}{E^m} & \frac{-\nu^m}{E^m} & \frac{1}{E^m} & 0 & 0 & 0 \\ 0 & 0 & 0 & \frac{1}{G^m} & 0 & 0 \\ 0 & 0 & 0 & 0 & \frac{1}{G^m} & 0 \\ 0 & 0 & 0 & 0 & 0 & \frac{1}{G^m} \end{bmatrix} \qquad \left(\underline{\underline{C}}^{f}\right)^{-1} = \begin{bmatrix} \frac{1}{E_t^f} & \frac{-\nu_t^f}{E_t^f} & \frac{-\nu_{tl}^f}{E_t^f} & 0 & 0 & 0 \\ \frac{-\nu_t^f}{E_t^f} & \frac{1}{E_t^f} & \frac{-\nu_{tl}^f}{E_t^f} & 0 & 0 & 0 \\ \frac{-\nu_{tl}^f}{E_l^f} & \frac{-\nu_{tl}^f}{E_l^f} & \frac{1}{E_l^f} & 0 & 0 & 0 \\ 0 & 0 & 0 & \frac{1}{G_{tt}^f} & 0 & 0 \\ 0 & 0 & 0 & 0 & \frac{1}{G_{tl}^f} & 0 \\ 0 & 0 & 0 & 0 & 0 & \frac{1}{G_{tl}^f} \end{bmatrix}$$

Vectors of induced strains in the constituents are: $\underline{\alpha}^m = \begin{bmatrix} \alpha^m \\ \alpha^m \\ \alpha^m \\ 0 \\ 0 \\ 0 \end{bmatrix}$ $\underline{\alpha}^f = \begin{bmatrix} \alpha_t^f \\ \alpha_t^f \\ \alpha_l^f \\ 0 \\ 0 \\ 0 \end{bmatrix}$

Mechanical behaviour of the wood material in the reference of microfibrils

The fibre wall can be considered as the superposition of two phases, both having a specific spatial organization. Crystalline material forms a framework of microfibrils oriented along direction *l*. Amorphous material can be considered as a continuous matrix with holes at the location of the crystalline cellulose. Behaviour of the wood material is approximated by a simple law of mixture of the two phases in volumetric proportions p_m and $p_f = 1-p_m$, so that:

$$\underline{\varepsilon}^{m+f} = \underline{\varepsilon}^{m} = \underline{\varepsilon}^{f} \tag{2}$$

$$\underline{\sigma}^{m+f} = p_m \underline{\sigma}^{m} + p_f \underline{\sigma}^{f} \tag{3}$$

The constitutive law is then:

$$\underline{\sigma}^{m+f} = p_m \underline{\underline{C}}^{m}(\underline{\varepsilon}^{m+f} - \underline{\alpha}^{m}) + p_f \underline{\underline{C}}^{f}(\underline{\varepsilon}^{m+f} - \underline{\alpha}^{f}) = \underline{\underline{C}}^{m+f}(\underline{\varepsilon}^{m+f} - \underline{\alpha}^{m+f}) \tag{4}$$

with: $\underline{\underline{C}}^{m+f} = p_m \underline{\underline{C}}^{m} + p_f \underline{\underline{C}}^{f}$ $\qquad \underline{\alpha}^{m+f} = (\underline{\underline{C}}^{m+f})^{-1}(p_m \underline{\underline{C}}^{m} \underline{\alpha}^{m} + p_f \underline{\underline{C}}^{f} \underline{\alpha}^{f})$

Mechanical behaviour of the wood material in the reference of the fibre

Microfibrils in the fibre wall are oriented at an given angle (MFA), noted ϕ, from the fibre longitudinal axis. Behaviour of wood material in the cylindrical reference of the fibre $r\theta z$ (z is the longitudinal axis of the fibre, r the radial and θ the tangential direction) can be deduced from that expressed in the *ttl* reference (denoted by numeric sub-scripts) using classical rotation formula (with $s = \sin\phi$ and $c = \cos\phi$):

$$C_{rr} = C_{11}$$

$$C_{\theta\theta} = c^4C_{22} + s^4C_{33} + 2c^2s^2C_{23} + 4c^2s^2C_{44}$$

$$C_{zz} = s^4C_{22} + c^4C_{33} + 2c^2s^2C_{23} + 4c^2s^2C_{44}$$

$$C_{z\theta} = C_{\theta z} = c^2s^2C_{22} + c^2s^2C_{33} + (c^4+s^4)C_{23} - 4c^2s^2C_{44}$$

$$C_{rz} = C_{zr} = c^2C_{31} + s^2C_{12}$$

$$C_{\theta r} = C_{r\theta} = s^2C_{31} + c^2C_{12}$$

$$C_{\rho r} = C_{r\rho} = csC_{31} - csC_{12}$$

$$C_{\rho\theta} = C_{\theta\rho} = -c^3sC_{22} + cs^3C_{33} + cs(c^2-s^2)C_{23} + 2cs(c^2-s^2)C_{44}$$

$$C_{\rho z} = C_{z\rho} = -cs^3C_{22} + c^3sC_{33} + cs(s^2-c^2)C_{23} + 2cs(s^2-c^2)C_{44}$$

$$C_{\rho\rho} = c^2s^2C_{22} + c^2s^2C_{33} - c^2s^2C_{23} + (c^2-s^2)^2C_{44}$$

$$C_{\tau\tau} = c^2C_{55} + s^2C_{66}$$

$$C_{\lambda\lambda} = s^2C_{55} + c^2C_{66}$$

$$C_{\lambda\tau} = C_{\tau\lambda} = scC_{55} - scC_{66}$$

$$\alpha_r = \alpha_1$$

$$\alpha_\theta = c^2\alpha_2 + s^2\alpha_3$$

$$\alpha_z = s^2\alpha_2 + c^2\alpha_3$$

$$\alpha_\rho = -2sc\alpha_2 + 2sc\alpha_3$$

Because of this rotation, new terms of coupling appear between normal strains and shear stress in the θz plane, and between shears in the rz plane and in the $r\theta$ plane. A term of θz shear also appears in the induced strains. Because of the anti-symmetric situation of adjacent cell walls, we assume that shear are fully restrained in the fibre wall. Then, behaviour of the fibre is sufficiently described by the stiffness matrix and strain vector reduced to their normal components.

Given the behaviour of elementary constituents, this models allow to compute all terms of $\underline{\underline{C}}$ and $\underline{\alpha}$ as functions of the proportion and orientation of the microfibril framework, p^f and ϕ.

Expression of the mechanical problem for a multi-layer cylinder

The mechanical problem consists of computing the displacement field $\underline{u} = (u_r, u_\theta, u_z)$ at equilibrium inside the fibre wall. Because of cylindrical symmetries, this field only depends on the radial position inside the fibre wall: $\underline{u} = \underline{u}(r)$. For the same reason, we make the assumption of generalized plane strains, so that the displacement along z does not depend on the radial position: $u_z(r) = z\varepsilon_z$, ε_z being the constant longitudinal strain. As we assumed full shear restraint, it comes that $u_\theta(r) = 0$. Then, the mechanical problem is reduced to the determination of $u_r(r)$ and ε_z. The field of radial strain is derived from the radial displacement: $\varepsilon_r = \mathrm{d}u_r/\mathrm{d}r = u_r'$ (5)

Cinematic compatibility inside a cylinder implies that: $\varepsilon_\theta = u_r/r$ (6)

Static equilibrium inside a cylinder implies that: $r\mathrm{d}\sigma_r/\mathrm{d}r + \sigma_r - \sigma_\theta = 0$ (7)

Mechanical behaviour of the material is given by: $\underline{\sigma} = \underline{\underline{C}}(\underline{\varepsilon} - \underline{\alpha})$ (8)

Injecting equations (5), (6) and (8) into (7), it comes that:

$$ru_r'' + u_r' - (C_{\theta\theta}/C_{rr})u_r/r = [\varepsilon_z(C_{\theta z} - C_{rz}) + \beta_\theta - \beta_r]/C_{rr} \quad (9)$$

with β_θ and β_r defined as the induced stress in the tangential and radial directions:

$$\beta_\theta = -C_{\theta r}\,\alpha_r - C_{\theta\theta}\,\alpha_\theta - C_{\theta z}\,\alpha_z \qquad \beta_r = -C_{rr}\,\alpha_r - C_{r\theta}\,\alpha_\theta - C_{rz}\,\alpha_z$$

Equation (9) in a second-order differential equation defining the equilibrium solution.

Analytical solution for a multi-layer=[-

Using the following notations:

$$\gamma^2 = C_{\theta\theta}/C_{rr} \qquad K_\beta = (\beta_\theta - \beta_r)/C_{rr} \qquad K_z = (C_{\theta z} - C_{rz})/C_{rr}$$

A general solution of this equation is (γ^2 and $K_\beta + K_z\varepsilon_z$ being uniforms, and assuming $\gamma \neq 1$):

$$u_r(r) = Ar^\gamma + Br^{-\gamma} + \varepsilon_z K_z/(1-\gamma^2) + rK_\beta/(1-\gamma^2) \quad (10)$$

The field of radial displacement can be calculated in each layer i using the above solution. The field of radial stress can be derived using equation (8). We define a_i, b_i, c_i, d_i, e_i, f_i, g_i, h_i, known functions of r so that, for $r \in [r_{i-1}, r_i]$:

$$u_r(r) = A_i a_i(r) + B_i b_i(r) + \varepsilon_z c_i(r) + d_i(r) \quad (11)$$

$$\sigma_r(r) = A_i e_i(r) + B_i f_i(r) + \varepsilon_z g_i(r) + h_i(r) \quad (12)$$

Explicit form of these functions is:

$$a_i(r) = r^{\gamma i} \qquad b_i(r) = r^{-\gamma i}$$

$$c_i(r) = K_{zi}/(1-\gamma_i^2) \qquad d_i(r) = rK_{\beta i}/(1-\gamma_i^2)$$

$$e_i(r) = (\gamma_i C^i_{rr} + C^i_{r\theta}) r^{\gamma i-1} \qquad f_i(r) = -(\gamma_i C^i_{rr} - C^i_{r\theta}) r^{-\gamma i-1}$$

$$g_i(r) = [(C^i_{rr} + C^i_{r\theta}) K_{zi}/(1-\gamma_i^2) + C^i_{rz}] \qquad h_i(r) = (C^i_{rr} + C^i_{r\theta}) K_{\beta i}/(1-\gamma_i^2) + \beta_r{}^i$$

For a structure with n layers, expressions defining u_r and σ_r contain $2n$ unknown integration constants (A_i and B_i) and the unknown longitudinal strain ε_z. These $2n+1$ unknown quantities are determined by interface and boundary conditions.

Interfaces between layers define continuity conditions for u_r and σ_r at r_i for $i \in [1, n-1]$:

$$u_r(r_i) = A_i a_i(r_i) + B_i b_i(r_i) + \varepsilon_z c_i(r_i) + d_i(r_i) = A_{i+1} a_{i+1}(r_i) + B_{i+1} b_{i+1}(r_i) + \varepsilon_z c_{i+1}(r_i) + d_{i+1}(r_i) \quad (13)$$

$$\sigma_r(r_i) = A_i e_i(r_i) + B_i f_i(r_i) + \varepsilon_z g_i(r_i) + h_i(r_i) = A_{i+1} e_{i+1}(r_i) + B_{i+1} f_{i+1}(r_i) + \varepsilon_z g_{i+1}(r_i) + h_{i+1}(r_i) \quad (14)$$

Boundary conditions

Boundary conditions of the fibre are defined in the transverse plane at its internal radius r_n and external radius r_0. The internal bound of the fibre is assumed unrestrained:

$$\sigma_r(r_n) = A_n e_n(r_n) + B_n f_n(r_n) + \varepsilon_z g_n(r_n) + h_n(r_n) = 0 \quad (15)$$

We consider 2 options at the external bound (either restrained or unrestrained in displacement):

$$u_r(r_0) = A_1 a_1(r_0) + B_1 b_1(r_0) + \varepsilon_z c_1(r_0) + d_1(r_0) = 0 \quad (16\text{-a})$$

or $$\sigma_r(r_0) = A_1 e_1(r_0) + B_1 f_1(r_0) + \varepsilon_z g_1(r_0) + h_1(r_0) = 0 \quad (16\text{-b})$$

For the longitudinal boundary condition, the same assumptions can be considered. The assumption of displacement restraint is simply expressed as: $\varepsilon_z = 0$ (17-a)

The fibre is stress-free at its longitudinal bound if the resultant axial load N (i.e. the sum of longitudinal stress) is null. This can be expressed as: (17-b)

With: $$j_i(r) = 2(\gamma_i C^i_{zr} + C^i_{z\theta}) r^{\gamma i+1}/(1+\gamma_i) \qquad k_i(r) = 2(-\gamma_i C^i_{zr} + C^i_{z\theta}) r^{-\gamma i+1}/(1-\gamma_i)$$

$$l_i(r) = [(C^i_{zr} + C^i_{z\theta}) K^i_z/(1-\gamma_i^2) + C^i_{zz}] r^2 \qquad m_i(r) = [(C^i_{zr} + C^i_{z\theta}) K^i_\beta/(1-\gamma_i^2) + \beta^i_z] r^2$$

Computation of stress and strain fields

Relations (13), (14), (15), (16), (17) form a linear system of $2n+1$ equations with $2n+1$ unknown quantities, from which the values of A_i, B_i and ε_z can be easily deduced. Fields of displacement, stress and strain are derived from them, using relations (5), (6), (8), (11) and (12).

The outputs of interest of the model are parameters describing the state of the fibre at its external bounds, namely $u_r(r_0)$, $\sigma_r(r_0)$, ε_z and N.